Small Pore Closure and the Deactivation of the Limestone Sulfation Reaction

The sulfation model of Simons and Rawlins (1980) is extended to include the effect of product deposits. The model includes: 1. the plugging of the smallest pores and the subsequent loss in the internal surface area, 2. the diffusion of the SO_2 through the product deposits, and 3. the loss of intraparticle diffusion due to the complete plugging of the largest pores. It is shown that the plugging of the smallest pores is generally rate-controlling.

G. A. Simons, A. R. Garman
Physical Sciences Inc.
Andover, MA 01810

SCOPE

Current sulfation models (Hartman and Coughlin, 1976, 1978; Bhatia and Perlmutter, 1981a,b; Christman and Edgar, 1983; Bardakci, 1984; Marsh and Ulrichson, 1982; Ramachandran and Smith, 1977) describe the intraparticle diffusion of SO_2 through porous CaO, the intrinsic kinetics of the $CaO + SO_2$ reaction, the buildup of the product layer ($CaSO_4$), the subsequent particle deactivation due to the relatively slow diffusion of SO_2 through the $CaSO_4$ to the unreacted CaO, and the ultimate termination of the reaction due to the plugging of the entire local porosity with the product deposits. These models are analyzed, and the results suggest an alternative deactivation mechanism: the plugging of the smallest pores and the associated loss in internal surface area. A pore-plugging model is developed that is compatible with a treelike description of pore branching (Simons, 1982). Product deposits systematically fill pores of all sizes, with the result that the entire local porosity is eventually plugged. The model is validated with both SO_2 and H_2S sorption data without invoking any adjustable parameters, such as the product layer diffusion coefficient. The model is readily available for parametric studies of the effect of sulfur concentration, particle size, porosity, internal surface area, and temperature on the calcium utilization achieved within specified time scales appropriate to various combustor or gasification devices.

CONCLUSIONS AND SIGNIFICANCE

The sorption of H_2S and SO_2 by a porous sorbent material (CaO) is described. The present model is distinct from previous models in its treatment of the role of the deposit layer, CaS for H_2S sorption and $CaSO_4$ for SO_2 sorption. The development of this product layer induces the deactivation of the sorbent particle. Previous models attribute this deactivation to diffusion through the product layer, whereas the present model attributes this deactivation to the plugging of the smallest pores and the subsequent loss of internal surface area. The plugging of small pores is validated by comparison of the present theory to data on BET surface evolution with sulfur sorption. The time-dependent sorbent model is validated by extensive comparisons with SO_2 and H_2S sorption data. The larger late time utilization of CaO by H_2S and the faster late time utilization rate are explained solely on the basis of the smaller molar volume of the product, CaS. The plugging of small pores simply occurs at higher CaO utilization and the utilization rate is not deactivated until the small pores are plugged. The model does not require an empirical fitting parameter, such as the product layer diffusion coefficient, that must vary with the reactant species and deposit product.

Correspondence concerning this paper should be addressed to G. A. Simons.

The model demonstrates that the initial porosity, internal surface area, diameter of the sorbent particle, and the molar volume of the product are the most important parameters in controlling sulfur sorption and CaO utilization. The internal surface area is rate-controlling for smaller particles, smaller product molar volumes, and at lower sorbent utilization (early time). The particle porosity is rate-controlling for larger particles, larger product molar volumes, and at larger sorbent utilization (late time). The model is capable of describing small, kinetically controlled particles with uniform sulfur deposition as well as large, diffusion-controlled particles with sulfur deposition only at the outer edge. The model may be applied to any reactive system so long as the intrinsic rate constant k_s has been measured. The value of k_s may be inferred from model-data comparisons in the limit of zero utilization, as in the case of H_2S and SO_2 (Simons and Rawlins, 1980).

Introduction

Limestone is a well-known and commonly used sorbent for SO_2 and H_2S. The limestone ($CaCO_3$) is calcined (heated to decompose into CO_2 and highly porous CaO), then sulfated. The sulfation step represents the complex coupling of chemical reactions with the mass transport through a time-varying porous structure. To understand this process, the effects of the reaction kinetics, intraparticle diffusion, and the role of the evolving sulfur product layer must be isolated and examined. Numerous studies have been directed toward this goal. Borgwardt and Harvey (1972) studied the rate of reaction of CaO with SO_2 in an oxygen-rich (with respect to SO_2) environment to form $CaSO_4$. Particle sizes were decreased until the measured rates were particle-size-independent, thus indicating kinetic control. The intrinsic reaction rate was determined by extrapolating data to zero utilization (no sulfur deposition). The rate constant at 1,250 K was determined to be 0.22 cm/s, or, in present units, 0.014 kg SO_2 adsorbed/s/m^2 of CaO internal surface per MPa SO_2 pressure. This intrinsic rate constant reflects the fact that the sulfation rate is first-order in SO_2 partial pressure and first-order in surface area.

The intrinsic rate constant has been integrated into a pore-structure/pore-transport model (Simons and Rawlins, 1980) to describe sulfur sorption in the limit of zero utilization for arbitrary particle size, porosity, internal surface area, and SO_2 partial pressure. The intrinsic rate and the model have been confirmed (Simons et al., 1984) over a wide range of particle sizes (1 μm–1mm) and SO_2 pressures (30 Pa–5 kPa). The analysis is valid only for CaO utilization less than 20%, above which the SO_2 sorption rates decreased dramatically due to the buildup of the $CaSO_4$ deposit layer.

The role of the $CaSO_4$ deposits on the sulfation process has been the subject of several investigations. The molar volume of $CaSO_4$ is sufficiently large that the pores of the CaO may completely plug prior to total CaO utilization. Complete pore plugging and the loss of porosity at the outer edge of the particle is the dominant cause of the deactivation of large sorbent particles *in fluidized bed* combustors. Models describing this process (Georgakis et al., 1979; Lee and Georgakis, 1981) are semiempirical in nature. More fundamental mechanistic models have been proposed by Hartman and Coughlin (1976, 1978), Bhatia and Perlmutter (1981a,b), Christman and Edgar (1983), Bardakci (1984), Marsh and Ulrichson (1982), and Ramachandran and Smith (1977). These models are very similar in that they treat the diffusion of the SO_2 through the porous structure, the development of the product layer, and the ultimate plugging of the porous structure. They also include an important intermediate step: the diffusion of the SO_2 through the product layer. The values of the product layer diffusion coefficient are obtained by fitting the model predictions to the sorption data. All models yield approximately the same results and the values quoted here are from Bhatia and Perlmutter (1981a) for the temperature range 923 to 1,253 K.

$$\text{Product Layer Diffusion: } D_p = 5 \times 10^{-6} e^{-14{,}000/T} \text{ m}^2/s$$

$$\text{Intrinsic Rate Constant: } k_s = A e^{-6{,}750/T}$$

$$\text{where } A \simeq 7 \frac{\text{kg SO}_2}{s \cdot \text{m}^2 \cdot \text{MPa SO}_2}.$$

Since Bhatia and Perlmutter report rates that are based on SO_2 concentration, the value of $A = 7$ based on SO_2 partial pressure is only approximate ($\pm 15\%$) over this temperature range. However, this 15% variation is relatively minor in the light of more recent work (Simons, et al., 1984; Simons and Garman, 1985) which tends to suggest that the preexponential factor of k_s is between 3 and 7, the lower limit being consistent with the rate measured by Borgwardt and Harvey (1972). Thus, all available measurements of k_s suggest $3 < A < 7$.

The diffusion through the product layer will be slower than the intrinsic kinetic rate k_s when $D_p[(\rho_G c)/\delta] < k_s(p_G c)$, where c is the SO_2 mass fraction, ρ_G is the gas density, p_G is the gas pressure, and δ is the thickness of the deposit layer. Expressing this criterion as a limit on δ, sulfation is diffusion-controlled when $\delta > (\rho_G D_p)/(k_s p_G)$, which corresponds to 10 nm at 1,400 K and 1 nm at 1,000 K. These values of δ suggest that there are potentially two problems with the concept of deactivation via product layer diffusion:

1. Bulk diffusion concepts are applied to product layers whose thickness is only a few monolayers of $CaSO_4$.
2. The values of δ are of the same magnitude as the minimum pore sizes. Hence, small-pore plugging would prevent the SO_2 from reaching the edge of the $CaSO_4$ layer.

If the product layer is uniformly distributed over the internal surface area s_p(m^2/kg of CaO), then the CaO utilization (u) corresponding to δ is written $u = \delta s_p M_{cs}/V_p$, where M_{cs} is the molar weight of the calcined stone (0.056 kg) and V_p is the molar volume of the $CaSO_4$ product (52 cm^3). The internal surface area is related to the radius of the smallest pore (r_{min}) by (Simons and Rawlins, 1980), $s_p \simeq (10^{-4}\text{ m}^3/\text{kg})/(r_{min})$, and the CaO utilization becomes $u \simeq (0.1)(\delta/r_{min})$.

Since sorbent deactivation occurs at utilizations of 10 to 20%, deactivation appears to correspond to $\delta = 0(r_{min})$. Hence, the plugging of small pores is a likely deactivation mechanism.

To describe this deactivation mechanism, $CaSO_4$ must completely fill the smallest pores while SO_2 continues to diffuse through the larger pores of the particle. Recent work by Bhatia (1985) and by Simons and Garman (1985) has respectively incorporated this phenomenon into the random pore model (Bhatia and Perlmutter, 1981b; Gavalas, 1980, 1981) and the pore tree model (Simons, 1982, 1983a) respectively. The primary differences between these models are discussed in the next section, and the salient features of the pore-tree/pore-transport model are illuminated. The pore-plugging model is developed and validated in the succeeding sections. The model successfully explains both SO_2 and H_2S sorption data without invoking an empirical fitting parameter (D_p) for each reactant species.

Pore Structure and Transport Model

The traditional approach of both the grain theory (Hartman and Coughlin, 1976, 1978) and the random-pore model (Bhatia and Perlmutter, 1981b) is to balance the bulk diffusion of a reactant gas through a porous media with the chemical reactions on the interior surface area. This is expressed as

$$\frac{1}{R^2}\frac{d}{dR}\left(D_e R^2 \frac{dc}{dR}\right) = -\eta s_p k c \qquad (1)$$

where R is the spherical coordinate of the sorbent particle, c is the mass fraction of the reactant gas, k is the effective kinetic rate, s_p is the internal surface area, η is a constant characterizing the conversion of units, and D_e is the effective bulk diffusion coefficient. (*k is used in lieu of k_s in order that k may be extended to explicitly include product layer diffusion.)

To determine D_e, it may be postulated that the gaseous diffusion coefficient (D) of species c is simply weighted by the open volume in the porous structure. Hence, $D_e = D(\theta/\tau)$, where θ is the porosity of the sorbent particle and τ is the tortuosity which accounts for the simple fact that the diffusive path length through the porous structure is greater than dR. Since τ must approach unity as $\theta \rightarrow 1$, it follows that $\tau = 1/\theta$.

This chemical/diffusive system may be integrated in time to predict the decrease in θ and the subsequent decrease in intraparticle diffusion with sulfation. However, since the porosity is contained predominantly in the largest pores and the internal surface area is predominantly in the smallest pores, Eq. 1 states that the diffusion occurs in the large pores while the chemical reaction occurs in the smallest pores. In reality, the chemical reaction occurs on the walls of the pores in which the reactant gas actually diffuses. This apparent paradox was formally addressed by Gavalas (1980, 1981). An equation equivalent to Eq. 1 may be written to express the balance between the diffusion of species c through a pore of radius r_p, and the chemical reaction on the walls of the pore. Integrating this equation over all pore sizes at fixed R, the value of D_e is expressed as an integral over all pore sizes. However, an immediate problem becomes evident. It is necessary to assume that all pores intersect and mix within the length scale dR. This leads to a contradiction: The kinetic activity in the large pore has explicit knowledge of the size of the smallest pores (Simons, 1983a). This is due to the high level of pore interconnectivity assumed in formally obtaining Eq. 1 as an integral over all pores.

To eliminate this problem, a treelike pore structure has been proposed (Simons, 1982). This structure is much less permeable than the traditional models. When applied to coal pyrolysis (Simons, 1983b, 1984), the resistance to bulk flow is a thousand times greater than that of random-pore models (Gavalas and Wilks, 1980). Key aspects of the pore tree theory, with respect to pore interconnectivity, have been validated for coal and char (Kothandaraman and Simons, 1984). Recognizing the similarity in the pore size distribution of char and calcine (Simons and Rawlins, 1980), the pore tree model is a viable tool with which small-pore plugging may be described in the sulfation process.

Following the pore structure theory of Simons (1982), consider a spherical particle of radius a containing pores of length ℓ_p and radius r_p. The pore dimensions range from a microscale, of the order of nanometers, to a macroscale that is a significant fraction of the particle radius. The radius of the largest pore is denoted by r_{max} and is given by $r_{max} = 2a\theta^{1/3}/3K_o$, where K_o is a constant of integration, approximately equal to 5, which relates the pore length to its radius $\ell_p = K_o r_p/\theta^{1/3}$. The radius of the smallest pore is denoted by r_{min} and is given by $r_{min} = 2\theta/\beta\rho_{cs}s_p$, where $\beta = \ln(r_{max}/r_{min})$, ρ_{cs} is the solid density of the calcined stone, and s_p is the specific internal surface area (typically of order 10^4 m^2/kg).

The particle contains a continuous distribution of pore sizes from r_{min} to r_{max}. The number of pores within an arbitrary cross section of area A and with radius between r_p and $r_p + dr_p$ is denoted by $\bar{g}(r_p)Adr_p$. The pore distribution function $\bar{g}(r_p)$ is given by $\bar{g}(r_p) = \theta/2\pi\beta r_p^3$, where $\bar{g}(r_p)$ indicates an average over all inclination angles between the axis of the pore and the normal to the plane. Due to the random orientation of the pores, the intersection of a circular cylinder with a plane is an ellipse of average area $2\pi r_p^2$. Hence the porosity is the $2\pi r_p^2$ moment of $\bar{g}(r_p)$ and the internal surface area is the $4\pi r_p$ moment of $\bar{g}(r_p)$. The expression for $\bar{g}(r_p)$ was derived from statistical arguments (Simons and Finson, 1979) and predicts that the pore volume between r_{min} and r_p increases linearly with the natural logarithm of r_p. It is the functional form of this relationship, $\int_{r_{min}}^{r_p} r_p^2\bar{g}(r_p)dr_p = \text{constant} \times \ln r_p$, that depicts the inverse cubic dependence of $\bar{g}(r_p)$ on r_p. A linear display of mercury intrusion volume (Simons, 1983a) always infers an Λ/r_p^3 distribution where Λ is specified by the pore volume and is proportional to the slope of the intrusion volume with respect to $\ln(r_p)$. This distribution function is compared to data for calcined limestone in Figure 1. Local variations in Λ may be rationalized as local errors in the pore radius, which is considerably more accurate than resorting to a bimodal or trimodal distribution function that incorporates all the pore volume into two or three distinct pore sizes.

Each pore that reaches the exterior surface of the sorbent particle is depicted as the trunk of a tree. The size distribution of tree trunks on the exterior surface of the particle is denoted by $\bar{g}(r_t)4\pi a^2 dr_t$ where $\bar{g}(r_t)$ is functionally identical to $\bar{g}(r_p)$. Each trunk of radius r_t is associated with a specific treelike structure, with continuous branching to ever-decreasing pore radii. The radius and number of pores is a unique function of the distance x into the tree. The coordinate x is skewed in that it follows a tortuous path through the branches of the tree. Let $n(x)$ represent the number of pores of radius r_p at location x in a tree of trunk radius r_t. An analysis (Simons, 1982) of this pore tree has demonstrated that $n(x) = r_t^2/r_p^2(x)$, and the coordinate x is related to r_p by $dr_p/dx = -r_p/\ell_t$.

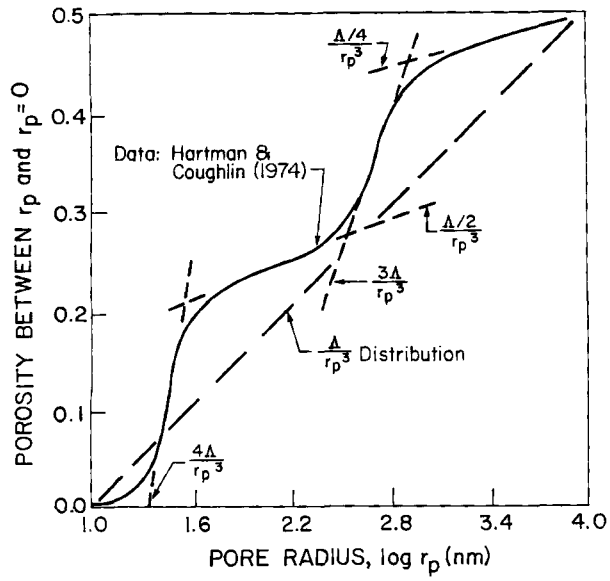

Figure 1. Pore size distribution in calcined limestone.

When this porous structure is placed in an SO_2 environment, SO_2 will diffuse into the pore tree and react with the CaO that constitutes the walls of the pores. The diffusion of SO_2 through n pores of radius r_p is balanced by the reaction of SO_2 at the walls of the pores. This is expressed as

$$\frac{d}{dx}\left(n\rho_G D\pi r_p^2 \frac{dc}{dx}\right) = n2\pi r_p k p_G \xi c \tag{2}$$

where c denotes the gaseous mass fraction of SO_2, ρ_G is the gas density within the pore, D is the self-diffusion coefficient of SO_2 in an arbitrary gaseous environment, k is the kinetic rate constant, and ξ is the ratio of the mole fraction of SO_2 to the mass fraction of SO_2.

The total sorption rate of the pore tree, $\dot{M}_t$, is related to the gradient of c at $x = 0$ by

$$\dot{M}_t = -\rho_G D\pi r_t^2 \frac{dc}{dx}\bigg|_0. \tag{3}$$

However, to obtain the value of dc/dx at $x = 0$, Eq. 2 must be integrated subject to the boundary conditions that $c = c_o$ at $x = 0 (r_p = r_t)$ and $dc/dx = 0$ at $x = x_t (r_p = r_{\min})$.

When the diffusion of SO_2 within the pore is dominated by gas-wall collisions, the corresponding Knudsen diffusion coefficient D is given by $D = (2/3)(\bar{V} r_p)$, where $\bar{V}$ is the mean thermal speed of an SO_2 molecule at the sorbent temperature and $2r_p$ is the mean free path between collisions with the walls. Within these restrictions, the total sulfation rate of the pore tree is obtained from Eq. 3 and the solution for the SO_2 concentration profile. In the limit of $r_t \gg r_{\min}$, $\dot{M}_t$ is expressed as

$$\dot{M}_t = \pi r_t^2 c_o \left(\frac{4\xi k p_G \rho_G \bar{V}}{3}\right)^{1/2} \left(\frac{e^{2\kappa} - 1}{e^{2\kappa} + 1}\right), \tag{4}$$

where

$$\kappa = \left(\frac{3\xi k p_G}{\rho_G \bar{V}}\right)^{1/2} \frac{S_t}{2\pi r_t^2}, \tag{5}$$

and S_t, the total surface area of the pore tree, is given by

$$S_t = 2\pi r_t \ell_t \left(\frac{r_t}{r_{\min}}\right)(1 - \theta). \tag{6}$$

Equation 4 clearly demonstrates two limits: for $\kappa > 1$, the Thiele (1939) diffusion solution (all species c consumed in tree trunk) is recovered, whereas for $\kappa < 1$, the sulfation rate is limited by the kinetic rate k acting on the total surface of the pore tree. No intermediate modes occur. Large trees (large κ) are diffusion-controlled, whereas small trees (small κ) are kinetically limited. For all practical purposes, $\dot{M}_t$ may be approximated by the kinetic solution for $\kappa < 1$ and by the diffusion solution for $\kappa > 1$. This approach was used to develop a transport model (Simons, 1979) for the char oxidation reaction. The transport model was generalized to include both Knudsen and continuum diffusion. The total sulfation rate of the sorbent particle is obtained by integrating $\dot{M}_t$ over all trees

$$\dot{M}_T = \int_{r_{\min}}^{r_{\max}} \dot{M}_t 4\pi a^2 \bar{g}(r_t) dr_t. \tag{7}$$

This model has been used to successfully describe sulfur sorption in the limit of zero utilization (Simons and Rawlins, 1980; Simons et al., 1984) and is extended to include $CaSO_4$ and CaS deposition in the next section.

Pore-Plugging Model

The transport model described in the preceding section is critically dependent on the radius of the smallest pore, as it is $r_{\min}$ that prescribes the internal surface area and the limits of integration over the pore trees (Eq. 7). As sulfur deposition occurs, the smallest pores will plug and the lower bound on the pore radius will increase in direct proportion to the thickness of the product layer, $\delta(t)$. The time-dependent minimum pore radius is expressed as

$$r_{\min}(t) = r_{\min}(o) + f\delta(t) \tag{8}$$

where f is a shape factor (to be determined) which reflects the fact that some of the product fills the volume previously occupied by the CaO and some grows into the void space.

The value of $\delta(t)$ is obtained by converting the mass sorption rate into a product layer growth rate and integrating over time

$$\frac{d\delta}{dt} = k p_G c_o \xi V_p / M_j \tag{9}$$

where V_p is the molar volume of the product ($CaSO_4$), M_j is the molar weight of the reactant species (SO_2), and c_o is the SO_2 mass concentration on the external surface of the sorbent particle. In Eq. 9, c_o has been used instead of the spatially dependent variable $c(x)$. This single value of δ (corresponding to $c = c_o$) applies and is used only where maximum sulfation occurs. This approximation satisfies both the limits of kinetic and diffu-

sion (in the pore) control. If a tree is kinetically controlled, the mass concentration in every pore is c_o. If the sulfation is controlled by Knudsen diffusion in the trunk, then c is c_o only in the trunk. Since there is little or no sulfation in the fine branches of a diffusionally controlled pore tree, neither δ nor the sulfation rates are calculated in this region of the pore tree. There will be a narrow range of tree sizes that lie in the transition regime between kinetic and diffusion control for which this approximation will yield only 50% accuracy (Simons, 1982). However, when integrating over all pore trees, this error will be insignificant and the resulting model will accurately describe both small, kinetically controlled particles as well as large, diffusion-controlled particles in which the sulfation occurs in a spherical shell near the exterior surface of the sorbent.

The one-dimensionality of the expression for δ may be justified via the same arguments. When $\delta \ll r_p$, the one-dimensional approximation is valid and when $\delta \gg r_p$, the pore is plugged and no sulfation occurs. Errors in the sulfation rate occur only in the pore size range that is at the onset of plugging. Any intricate geometrical description of this pore-plugging process would not be justified because perfectly cylindrical pores do not exist, and because it would not significantly influence the net sulfation rate (integral over all pores).

The effective kinetic rate k is the rate that corresponds to the species concentration c in the pore, whereas k_s is the rate that corresponds to the actual concentration c_w on the CaO side of the deposit layer. To determine c_w, the diffusion of SO_2 through the product layer is balanced with the intrinsic kinetic rate k_s reacting with concentration c_w on the CaO side of the layer: $\rho_G D_p (c - c_w)/\delta = k_s p_G c_w \xi$. Solving for c_w/c, the effective kinetic rate is expressed as:

$$k = k_s\left(\frac{c_w}{c}\right) = k_s\left(1 + \frac{\xi k_s p_G \delta}{\rho_G D_p}\right)^{-1}. \tag{10}$$

Equations 8–10 are so constructed as to be immediately implemented into the pore structure/transport model, Eqs. 4–7, and numerically integrated with time. The CaO utilization rate becomes

$$\frac{du}{dt} = \frac{\dot{M}_T M_{cs}/M_j}{4/3\,\pi a^3 \rho_{cs}(1-\theta)} \tag{11}$$

where the numerator is the mass of CaO utilized per second and the denominator is the initial mass of CaO.

The determination of the shape fator f is the final step in the development of the pore-plugging model. To obtain f, Eq. 11 is expressed in the limit of kinetic control ($\kappa \ll 1$):

$$\frac{du}{dt} = \frac{2\theta \xi k p_G c_o V_{cs}}{\beta r_{\min} M_j}$$

Dividing Eq. 9 by du/dt yields

$$\frac{d\delta}{du} = \frac{\beta r_{\min}(t) V_p}{2\theta V_{cs}},$$

and substituting Eq. 8 into $d\delta/du$, integrating subject to $u = o$ at $\delta = 0$, $u(t)$ becomes $u(t) = (2\theta V_{cs}/f\beta V_p)\ln[r_{\min}(t)/r_{\min}(o)]$, where θ infers $\theta(u = o)$. As $r_{\min}(t) \to r_{\max}$, all pores are plugged and $u(t) \to u_{\max}$. Thus, f must be chosen such that $f \equiv (2\theta V_{cs}/V_p u_{\max})$.

The limit on CaO utilization ($u_{\max}$) may be thought of as a local characteristic (outer shell of a diffusion-limited particle) or as a homogeneous property (in kinetic control). This limit occurs because the molar volume of the deposit product is sufficiently large that all pores may plug before $u \to 1$. Consider one mole of calcined stone. The molar volume is V_{cs}, the bulk volume is V_B, and the initial porosity is $\theta = (V_B - V_{cs})/V_B$.

As V_{cs} is converted to a sulfate product (molar volume V_p), $\theta(u)$ is V_B less the volume of the unreacted calcine less the volume of the reacted product: $\theta(u) = [V_B - V_{cs}(1-u) - uV_p]/V_B$.

The value of $u_{\max}$ corresponds to that of u at $\theta(u) = 0$:

$$u_{\max} = \frac{\theta}{(1-\theta)}\frac{V_{cs}}{(V_p - V_{cs})}$$

and the shape factor f becomes

$$f = 2(1-\theta)\frac{V_p - V_{cs}}{V_p} \tag{12}$$

Note that δ expands into the pore only when the product volume is greater than the volume of CaO. Also, the higher the local porosity, the less growth there will be into any one pore. This is due to pore overlap, or more precisely, the overlap in the product layers of each pore.

The values of $u_{\max}$ for the cases of SO_2 and H_2S reacting with CaO are illustrated in Figure 2. The CaO utilization is extremely sensitive to the porosity. Since the porosity of the calcined stone may readily be between 0.5 and 0.8 (Hartman and Coughlin, 1978), the derivation of f must be extended to include the case where $u \to 1$ for $\theta(1) \neq 0$. From the pore structure model (Simons, 1982), $\theta(1) = \theta \ln[r_{\max}/r_{\min}(t)]/\beta$, and since $\theta(1) = (V_B - V_p)/V_B$, $u(t) = 1$ if and only if f is given by Eq. 12. Hence, the formulation is completely general and may be applied to any sorpotion system.

In applying the model to a sorption process where $V_p \to V_{cs}$,

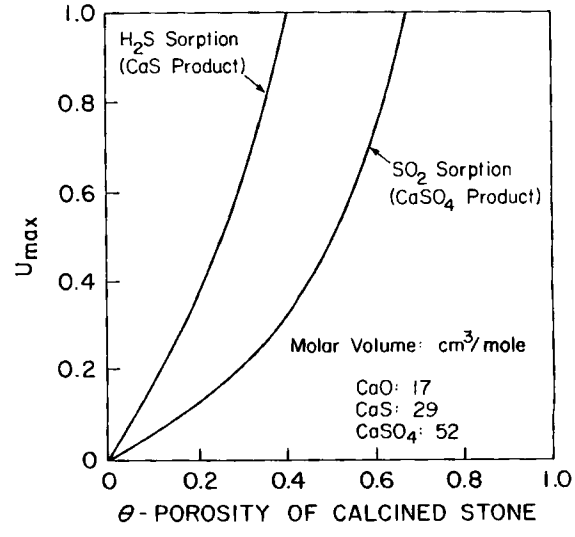

Figure 2. Maximum utilization of the CaO.

the shape factor f is zero, pore plugging cannot occur, and the sorpotion reaction will not terminate until all of the sorbent is utilized. This limit is implemented in the formulation by incorporating the requirement that the net reaction rate must decrease in direct proportion to the remaining sorbent $(1 - u)$, independent of pore plugging or product layer diffusion. This is most readily accomplished by incorporating the $(1 - u)$ into k_s. Hence, k_s is expressed as $k_s = A(1 - u)e^{-6,750/T}$.

Model Validation

The pore-plugging model may be validated by comparison with sulfation data taken over a wide range of test conditions. The sulfation experiments of Borgwardt and Harvey (1972) were conducted using 3×10^{-5} kg of 96 μm dia. CaO particles in simulated flue gas at 1,253 K. The comparison of the data with the theory is illustrated in Figures 3 through 5. Note that in absence of the limitations due to product layer diffusion (i.e., $D_p = \infty$), the intrinsic kinetics coupled with the pore-plugging model successfully explain the data. The scatter in the net reaction data is within the accuracy to which the intrinsic rate constant has been previously measured $(3 < A < 7)$. Note also that the sulfation rate is very sensitive to the porosity of the calcined stone. Type 4 ($\theta = 0.52$) is slightly more reactive than type 1 ($\theta = 0.45$), even though type 1 has considerably more internal surface area. Type 11 ($\theta = 0.80$) is much more reactive than type 4. This sensitivity to porosity was illustrated in Figure 2 and is a consequence of pore plugging. The reaction rates of smaller particles will be shown to be kinetically controlled and sensitive to the internal surface area as well. Thus, the porosity, internal surface area, and particle size must be well-characterized experimentally. Borgwardt and Harvey (1972) illustrated additional sulfation data as a function of particle size and internal surface area. However, the porosity of these samples was not characterized and comparisons with the model would not be meaningful.

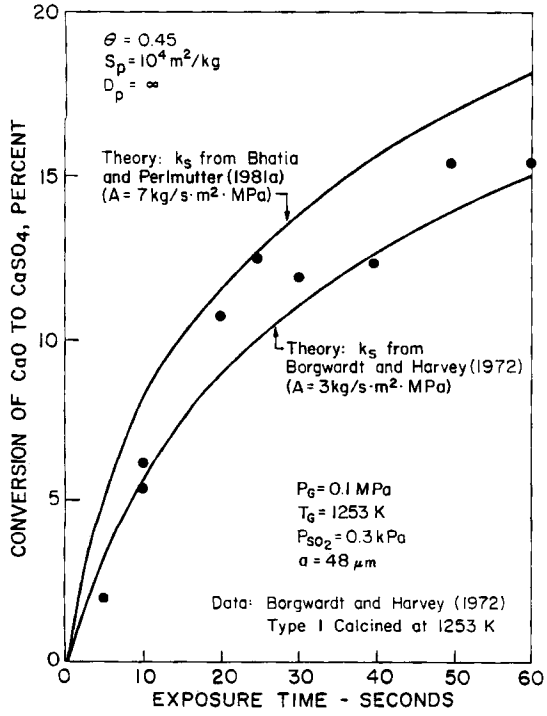

Figure 3. Model validation for 45% porous calcine.

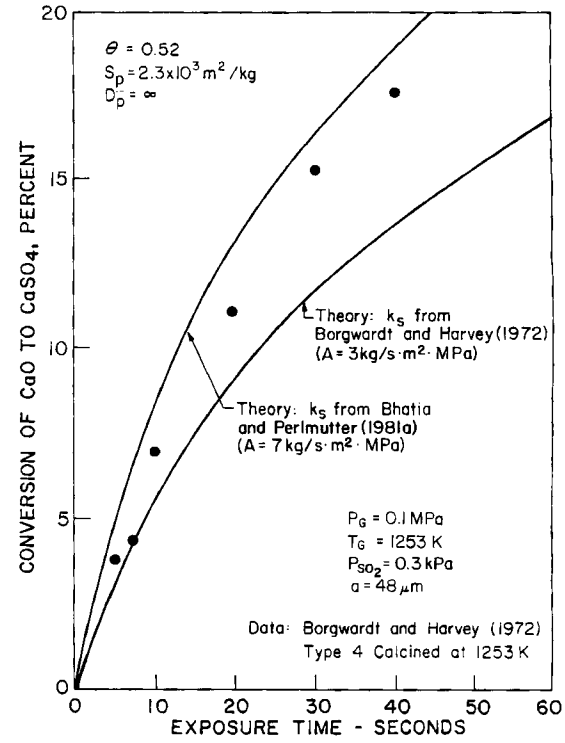

Figure 4. Model validation for 52% porous calcine.

Empirical validation of the plugging of small pores is directly demonstrated via BET surface area measurements on sulfated sorbent particles as a function of utilization (Roman et al., 1984). The surface area, Eq. 6, in the small trees ($\kappa < 1$) is characterized by $r_{min}(t)$, whereas that in the large trees ($\kappa > 1$) is

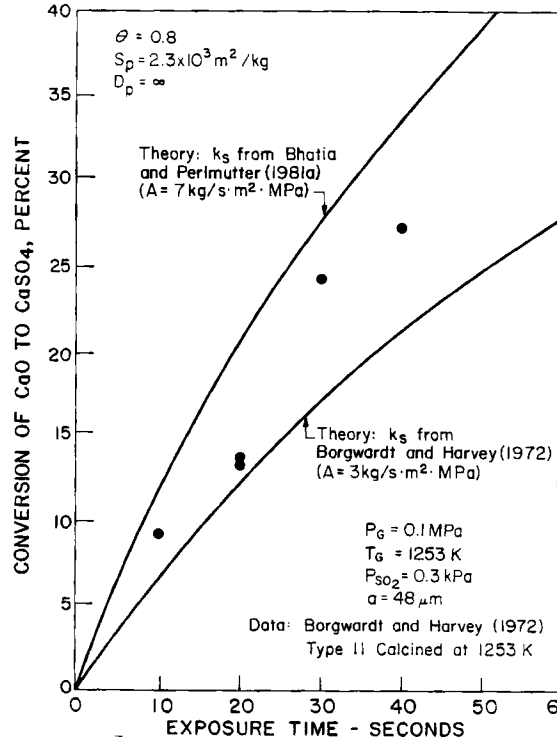

Figure 5. Model validation for 80% porous calcine.

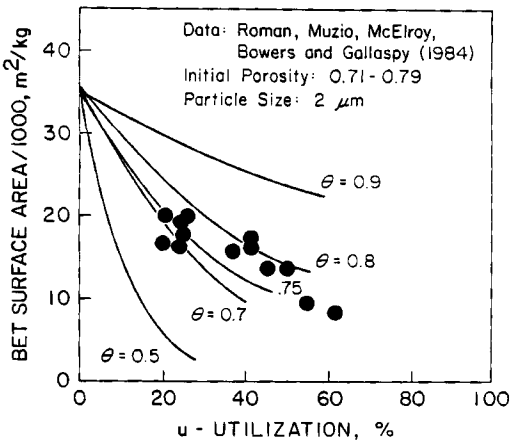

Figure 6. Decrease in surface area during sulfation.

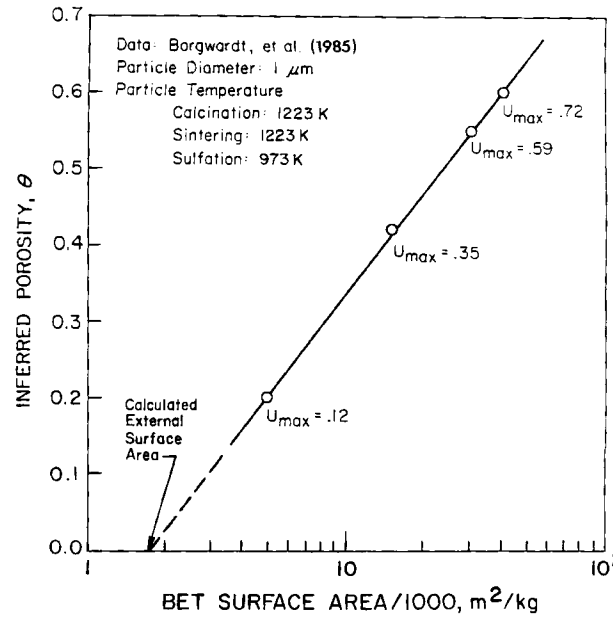

Figure 7. Sorbent porosity inferred from CaO utilization.

characterized by $r_{min}(o)$. This is a consequence of the sulfation occuring only in the trunks of the large trees while the BET gas adsorption will penetrate the small pores, $r_{min}(o)$. To account for the possibility that the tree trunk may be plugged, integrations include only those trees whose trunk size r_t lies between $r_{min(t)}$ and r_{max}. Internal surface area vs. utilization is generated from the sulfation model and compared to data in Figure 6. Calculated values of s_p are illustrated parametrically in θ. Measured values of θ lie between 0.71 and 0.79. The validity of the model is clearly illustrated by the data comparison. The ability of the model to accurately predict surface area evolution (small-pore plugging) is critical to the analysis of sulfation data on small (1 μm dia.) particles that are kinetically controlled.

Sorption data for 1 to 2 μm calcine particles has been obtained by Borgwardt et al. (1984, 1985). Limestone particles were calcined at moderate temperatures to form high internal surface area (80×10^3 m^2/kg) calcine, then sintered for several minutes to reduce the internal surface area. In this way, calcine particles of varying internal surface areas were developed. It is reasonable to expect that sintering will also change the porosity. However, no porosity data are available and porosity must be inferred indirectly. The sorption of SO_2 by these sintered particles illustrates (Borgwardt et al., 1985) an asymptote in the CaO utilization vs. time curve. These data imply u_{max} as a function of the internal surface area of the sintered particle. Relating u_{max} to porosity from Figure 2, a relationship between θ and s_p is deduced and illustrated in Figure 7. In this manner, the calcine particles are characterized in terms of both the internal surface area and the porosity.

Figure 7 suggests a very large reduction in both surface area and porosity with sintering. The reduction in surface area was achieved by sintering at 1,223 K for up to 2,000 s (Borgwardt et al., 1985). To verify the concept of reduced porosity, we have sintered the identical limestone (Fredonia, obtained from Borgwardt) at 1,223 K in a fixed-bed reactor for up to 2,000 s. Mercury porosimetry was used to determine the reduction in porosity with sintering time. However, the particle size used in these experiments was 100 μm, two orders of magnitude greater than the size studied by Borgwardt. Consequently, we measured only that porosity contained in pores whose size is characteristic of 1 μm particles. Figure 8 illustrates the porosity in pores of diame-

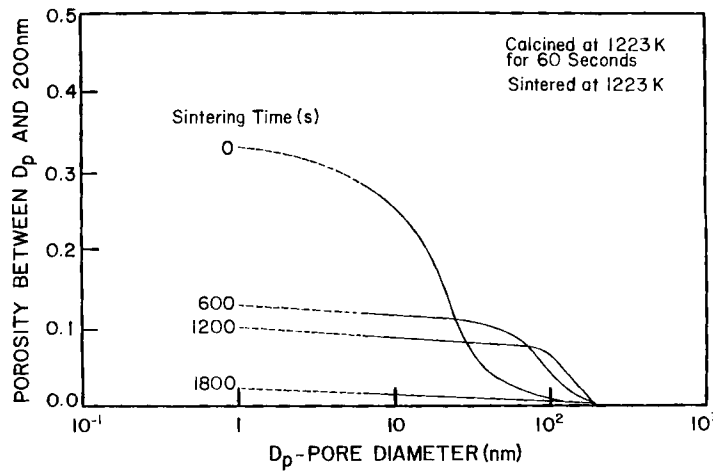

Figure 8. Porosity reduction with sintering time.

ter less than 200 nm. After calcination and prior to sintering, the pore volume between 1 and 200 nm dia. pores is 1.65×10^{-4} m^3/kg. For a sample with a bulk specific gravity of 2, this pore volume translates into a porosity of 33% (pore volume/bulk volume). Note that the dominant porosity lies in the 10–30 nm size range. As sintering proceeds, the porosity is totally removed from the small pores, shifts to the 100 nm pores at 600 to 1,200 s, and ultimately collapses at 1,800 s. The total porosity in the 1 to 200 nm dia. size range decreases monotonically with increased sintering time until a 1 μm dia. porous particle would collapse into a solid pellet after 1,800 s. This is also implied by Figure 7. Extrapolation of the s_p v. θ data to $\theta = 0$ implies $s_p \simeq 1.8 \times 10^3$ m^2/kg, which is the external surface area of a 1 μm dia. CaO pellet (specific gravity = 3.32). Hence, both sets of data imply total collapse of the pore structure with sintering. These surface area vs. porosity data are critical in explaining the sulfation data for these sintered particles.

The model is compared to the sulfation data for these sintered particles (Borgwardt et al., 1985) in Figure 9. The data were taken in a differential-flow reactor using CaO samples of the order of 10^{-5} kg, the temperature fixed at 973 K, and the O_2 mole fraction (5%) and the SO_2 mole fraction (3,000 ppm) typical of coal-fired boilers. The model predictions are superimposed on the data and illustrate excellent agreement for surface areas over the 5×10^3 to 50×10^3 m^2/kg range, corresponding to porosities of 20 to 60% inferred from Figure 7. The early-time

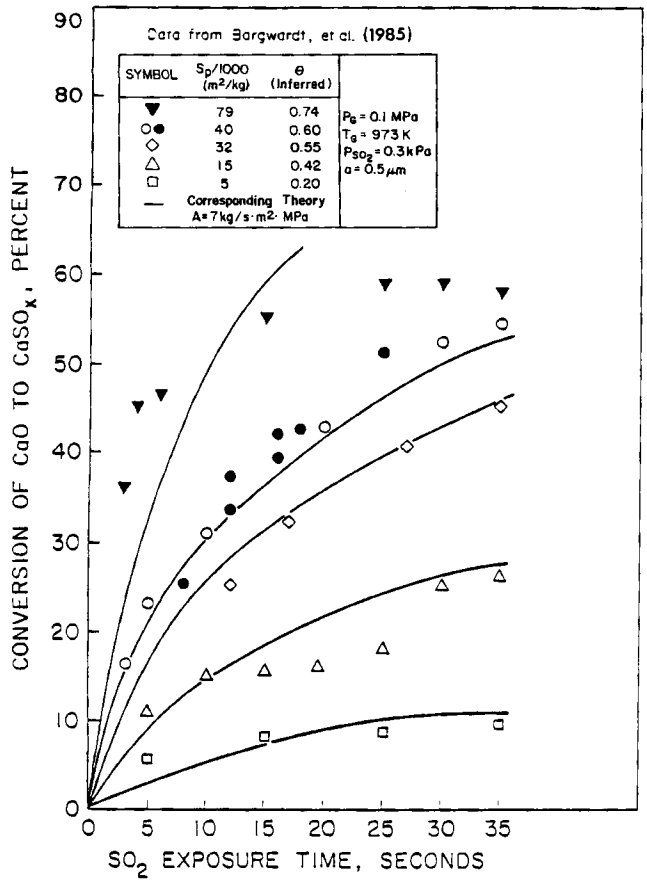

Figure 9. Model validation of the SO_2-CaO reaction.

$A = 7$. Variable surface area and porosity (inferred from maximum utilization).

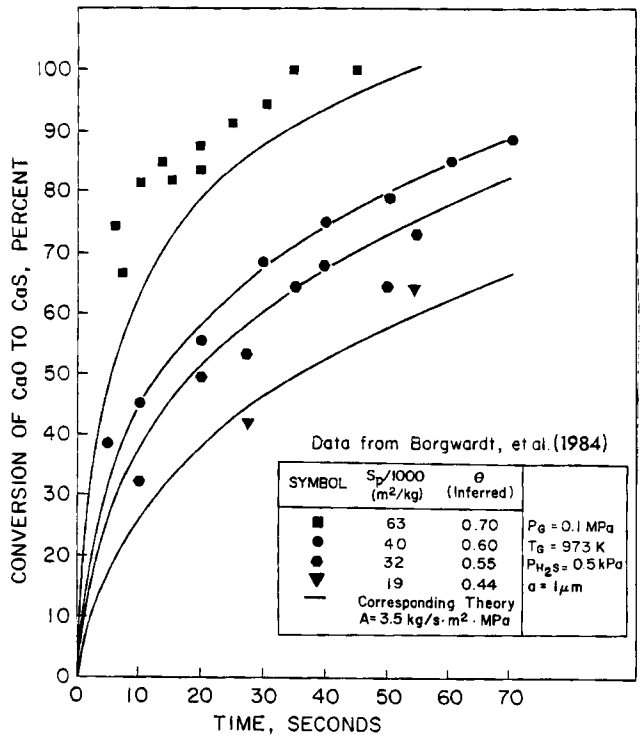

Figure 10. Model validation of the H_2S-CaO Reaction.

$A = 3.5$. Variable surface area and porosity (inferred from maximum utilization).

reactivity, which is kinetically limited, scales directly with surface area while the late-time reactivity, which is pore-plugging limited, is highly dependent on porosity. Agreement is least accurate for the highest specific surface area (79×10^3 m^2/kg). which is expected since the corresponding porosity is inferred from extrapolation of the porosity-surface area correlation beyond the range of available u_{max} data.

A critical test of the pore-plugging deactivation model is its ability to predict the H_2S-CaO reaction. The molar volume of the CaS product, 29 cm^3/mol, is nearly half that of $CaSO_4$. As a result, calcium utilization of 100% is possible for initial particle porosities greater than 42%. Figure 10 illustrates the data of Borgwardt et al. (1984) for 2 μm CaO particles reacted with H_2S. Variable surface areas were produced as described above by sintering over variable time scales. The initial porosity was inferred from the surface area-porosity relationship of Figure 7. The intrinsic H_2S reaction rate was fixed at one-half of the SO_2 rate ($A = 3.5$) as determined previously by Simons and Rawlins (1980). Again, the data validate the pore-plugging model, in addition to supporting the transient surface area-porosity relationship that developed during sintering.

Acknowledgment

This work was supported in part by the U.S. Department of Energy, Morgantown Energy Technology Center, Contract No. DE-RA21-84MC21388, and by Southern Company Services and the Electric Power Research Institute under Contract No. 195-84-022, and by Energy and Environmental Research Corporation and Pittsburgh Energy Technology Center under Contract No. 8538-2.

Notation

a = radius of sorbent particle
c = mass fraction of reactant gas in pore

c_o = mass fraction of reactant gas at exterior surface of particle
c_w = mass fraction of reactant gas at CaO surface
D = self diffusion coefficient of reactant gas
D_e = effective bulk diffusion coefficient
D_p = product layer diffusion coefficient
f = shape factor, Eq. 8
$\bar{g}(r_p)$ = pore distribution function
k_s = intrinsic kinetic rate constant: mass of reactant gas/area-time-SO_2 pressure
k = effective kinetic rate constant, k_s adjusted to include D_p
K_o = constant ≈ ratio of pore length to dia. ≈ 5 for pore tree
ℓ_p = length of pore radius r_p
ℓ_t = length of the pore that represents the trunk of a tree
M_{cs} = molar weight of calcined sorbent
M_j = molar weight of reactant gas
M_p = molar weight of deposit product
M_t = sulfation rate per pore tree
M_T = total sulfation rate of particle
$n(x)$ = number of pores of radius r_p at distance x into pore tree
p_G = gas pressure in pores
r_p = radius of pore
r_{min} = radius of smallest pore
r_{max} = radius of largest pore
r_t = radius of the pore that represents the trunk of a tree
R = spherical coordinate of porous particle
S_t = surface area of a pore tree
s_p = specific internal surface area (area/mass)
t = time
T = temperature of particle and gas in pores, K
u = utilization of sorbent, molar fraction
u_{max} = maximum local value of utilization
$\bar{V}$ = mean thermal speed of a molecule
V_B = bulk volume of one mole of porous calcined sorbent
V_{cs} = molar volume of calcined sorbent
V_p = molar volume of deposit product
x = skewed distance into pore or pore tree

Greek letters

β = $\ln(r_{max}/r_{min})$
δ = thickness of product layer
θ = initial porosity of calcined sorbent
κ = Eq. 5: $\kappa < 1 \rightarrow$ kinetic control
ξ = species mole fraction/species mass fraction
ρ_G = gas density
ρ_{cs} = nonporous density of calcined sorbent
θ = tortuosity

Literature cited

Bardakci, T., "Diffusional Study of the Reaction of Sulfur Dioxide with Reactive Porous Matrices," *Thermochimica Acta*, **76**, 287 (1984).

Bhatia, S. K., "Analysis of Distributed Pore Closure in Gas-Solid Reactions," *AIChE J.*, **31**, 642 (1985).

Bhatia, S. K., and D. D. Perlmutter, "The Effect of Pore Structure on Fluid-Solid Reactions. I: Application to the SO_2-Lime Reaction," *AIChE J.*, **27**, 226 (1981a).

———, "A Random-Pore Model for Fluid-Solid Reactions. II: Diffusion and Transport Effects," *AIChE J.*, **27**, 247 (1981b).

Borgwardt, R. W., and R. D. Harvey, "Properties of Carbonate Rocks Related to SO_2 Reactivity," *Environ. Sci. Technol.*, *6*, 350 (1972).

Borgwardt, R. H., N. F. Roache, and K. R. Bruce, "Surface Area of Calcium Oxide and Kinetics of Calcium Sulfide Formation," *Environ. Prog.*, **3**, 129 (1984).

———, "Method for Variation of Grain Size in Studies of Gas-Solid Reactions Involving CaO," Submitted to *I&EC Fundam.* (1985).

Christman, P. G., and T. F. Edgar, "Distributed Pore-Size Model for Sulfation of Limestone," *AIChE J.*, **29**, 388 (1983).

Gavalas, G. R., "A Random Capillary Model with Application to Char Gasification at Chemically Controlled Rates," *AIChE J.*, **26**, 577 (1980).

———, "Analysis of Char Combustion Including the Effect of Pore Enlargement," *Comb. Sci. Tech.*, **24**, 197 (1981).

Gavalas, G. R., and K. A. Wilks, "Intraparticle Mass Transfer in Coal Pyrolysis," *AIChE J.*, **26**, 201 (1980).

Georgakis, C., C. W. Chang, and J. Szekely, "A Changing Grain Size Model for Gas-Solid Reactions," *Chem. Eng. Sci.*, **34**, 1072 (1979).

Hartman, M., and R. W. Coughlin, "Reaction of Sulfur Dioxide with Limestone and the Influence of Pore Structure," *Ind. Eng. Chem. Proc. Des. Develop.*, **13**, 248 (1974).

———, "Reaction of Sulfur Dioxide with Limestone and the Grain Model," *AIChE J.*, **22**, 490 (1976).

———, "Influence of Porosity of Calcium Carbonates on Their Reactivity with Sulfur Dioxide," *Ind. Eng. Chem. Process Des. Dev.* **17**, 411 (1978).

Kothandaraman, G., and G. A. Simons, "Evolution of the Pore Structure in PSOC 140 Lignite During Pryoslysis," *20th Int. Symp.* Combust., Combustion Inst. (1984).

Lee, D. C., and C. Georgakis, "A Single-Particle Size Model for Sulfur Retention in Fluidized Bed Coal Combustors," *AIChE J.*, **27**(3), 472 (1981).

Marsh, D. W., and D. L. Ulrichson, "Rate and Diffusional Study of the Reaction of Calcium Oxide with Sulfur Dioxide," *AIChE Ann. Meet.*, Los Angeles (1982).

Ramachandran, P. A., and J. M. Smith, "A Single-Pore Model for Gas-Solid Noncatalytic Reactions," *AIChE J.*, **23**, 353 (1977).

Roman, V. P., L. J. Muzio, M. W. McElroy, K. W. Bowers, and D. T. Gallaspy, "Flow Reactor Study of Calcination and Sulfation," Paper No. 2B, *1st Joint EPRI/EPA Symp. Dry* SO_2 *and Simultaneous* SO_2/NO_X *Control Technol.*, San Diego (1984).

Simons, G. A., "Char Gasification. Part I: Transport Model," *Comb. Sci. Tech.*, **20**, 107 (1979).

———, "The Pore Tree Structure of Porous Char," *19th Int. Symp. Combustion*, Combustion Institute (1982).

———, "The Role of Pore Structure in Coal Pyrolysis and Gasification," *Prog. Energy Combust. Sci.*, **9**, 269 (1983a).

———, "The Influence of Fluid Transport During Pyrolysis," *Proc. 1983 Int. Conf. Coal Sci.*, Pittsburgh (1983b).

———, "Coal Pyrolysis. II: Species Transport Theory," *Combust. and Flame*, **55**, 181 (1984).

Simons, G. A., and M. L. Finson, "The Structure of Coal Char. I: Pore Branching," *Comb. Sci. Tech.*, **19**, 217 (1979).

Simons, G. A., A. R. Garman, and A. A. Boni, "High-Pressure Sulfur Sorption by Limestone," Paper No. 33, *East. Sec. Combust. Inst., Fall Tech. Meet.*, Clearwater Beach, FL (1984).

Simons, G. A., and A. R. Garman, "Intraparticle Mass Transfer During Sulfation by Calcined Limestone," *23rd AIChE/ASME Nat. Heat Trans. Conf.*, Denver (1985).

Simons, G. A., and W. T. Rawlins, "The Reacton of Sulfur Dioxide and Hydrogen Sulfide with Porous Calcined Limestone," *Ind. Eng. Chem. Process Des. Dev.*, **19**, 565 (1980).

Thiele, E. W., "Relation between Catalytic Activity and Size of Particle," *Ind. Eng. Chem.*, **31**, 916 (1983).

Manuscript received June 11, 1985, and revision received Dec. 17, 1985.